Ocean Engineering 89 (2014) 157–172

Contents lists available at ScienceDirect

Ocean Engineering

journal homepage: www.elsevier.com/locate/oceaneng

Flushing ballast tanks

Zhixin Qi*, Ian Eames, Alistair Greig

University College London, Torrington Place, London WC1E 7JE, UK

ARTICLE INFO

Article history:
Received 7 May 2013
Accepted 30 July 2014
Available online 28 August 2014

Keywords:
Ballast water
Flushing efficiency
Fluid mixing
Multi-compartment tank

ABSTRACT

The International Maritime Organization requires ballast water tanks to be flushed through with three tank volumes to remove aquatic species. We apply a network model for multiply connected compartments to analyse the influence of internal geometry and inlet–outlet positions on how much of the initial water of each compartment is flushed in time. A complementary experimental study was undertaken to quantify the flushing from 2×2, 3×3 and 5×4 tank configurations by an optical method. The agreement between the predictions and measurements is good. The results show that the flushing in a multi-compartment tank is generally more efficient than perfect mixing. The 95% reduction is met after three exchange volumes in all cases. The outlet needs to be positioned far from the inlet to reduce bypassing through the tank. These results are finally discussed in the context of international regulations for flushing ballast tanks.

1. Introduction

The largest fraction of the world's trade is transported by ships with estimates varying from 66% to 80% (see Wright and Mackey, 2006). Ballast is essential for the safe operation of ships; it ensures stability, trim, and structural integrity by maintaining shear stresses and bending moments within acceptable limits. The ballast on most ships is usually achieved using water, and the amount of ballast water transferred globally each year is estimated to be 10 billion tonnes (see Wright and Mackey, 2006; MacPhee, 2006). Ships usually discharge ballast water in ports while loading and take up ballast water in destination ports while unloading, where the water is shallow and rich in aquatic organisms. Taking up non-indigenous species (NIS) in one port and transporting them to another sea can lead to significant environmental problems. Zebra mussels, native to the Caspian Sea region of Asia but transported to the Great Lakes via ballast water, reduce the amount of phytoplankton available for other organisms and cost $100 M/year to manage control measures (see Pimentel et al., 2000). In order to prevent the transfer of aquatic organisms from one region to another via ballast water, the International Maritime Organization adopted the Ballast Water Management Convention in 2004. According to Ballast Water Exchange Standard, Regulation D-1 of the Convention, ships utilising the exchange method need to exchange ballast water at least 95% by volume; for ships exchanging ballast water by the pumping-through method, pumping through three times the volume of each ballast tank was considered to meet the standard. Pumping through less than three times the volume may be acceptable if the procedure can demonstrate that at least 95% of original ballast water is removed.

The original intention of the Ballast Water Convention was that the water exchange technique would be a short-term solution and be replaced by water treatment. When the Convention was written no ballast water treatment plants were in production. Their development has been slower than expected due to various reasons including an underestimation of the technical challenges, insufficient resources and market economics (see King et al., 2012). The magnitude of the logistical effort required for effective enforcement and regulation of various aspects of the Convention have also been identified as potential barriers to implementation (see Wright, 2012). These are some of the reasons that the Convention is still not ratified even though some of its initial deadlines for implementation have already passed. The situation is complex but the outcome is that ballast water exchange is still in widespread use and will continue to be so for quite some time. Moreover some authorities are now insisting on a combination of ballast water exchange and treatment. It is also becoming clear that a much more detailed understanding of the flow behaviour within ballast tanks is required for compliance assessment and enforcement once ballast water treatment is introduced.

Ballast tank designs are currently driven entirely by structural considerations of the vessel, customised for maximum cargo capacity and practicality of human access and construction. The tanks are structurally complex and composed of interconnected bays, longitudinal and transverse stringers/stiffeners to improve the strength of the vessel. The usual layout of ballast tanks on a bulk carrier consists of the tanks located at the fore peak, aft peak,

* Correspondence to: Mechanical Engineering, University College London, Torrington Place, London WC1E 7JE, UK.
E-mail address: zhixin.qi.10@ucl.ac.uk (Z. Qi).

http://dx.doi.org/10.1016/j.oceaneng.2014.07.022

upper/topside wing, lower/hopper wing and bottom. The double bottom tank and hopper tank are unified and in some cases are connected with the upper wing/topside tanks by a trunk that allows the ballast water to flow between them. Fig. 1 shows a schematic of the ballast tanks of a bulk carrier. Other tankers have slimmer ballast water tanks along the ship and do not alternate. These ballast tanks are large with a simple box design, and have a capacity of 40,500 m^3 of water serviced by pumps with a flow rate of 3000 m^3/h (or $\sim 1\ m^3/s$).

Inside the double bottom tank, individual compartments are generated by crossing longitudinal and transverse stiffeners and frames with lightening holes. The neighbouring compartments are associated with lightening holes, stringers and limber holes, shown in Fig. 2. The ballast tank flushing is achieved either from the inlet as shown in Fig. 1(b) by the sequential (empty/refill) method or through overflow arrangements by the flow through method. For the flow-through method, the overflow is achieved from two air/sounding pipes either on the deck or to the side, typically with a diameter of 0.15–0.2 m.

The NIS that can be drawn into a ballast tank range from bacteria, plankton, fish eggs or crabs to fish (see Wonham and Carlton, 2005). Associated with these is a settling or swimming velocity, ranging from 0.1 to 150 mm/s (see Wong and Piedrahita, 2000; Magill et al., 2006). The smaller species are essentially advected with the flow and can be regarded as essentially passive during flushing. When the species are passive, the fraction of the

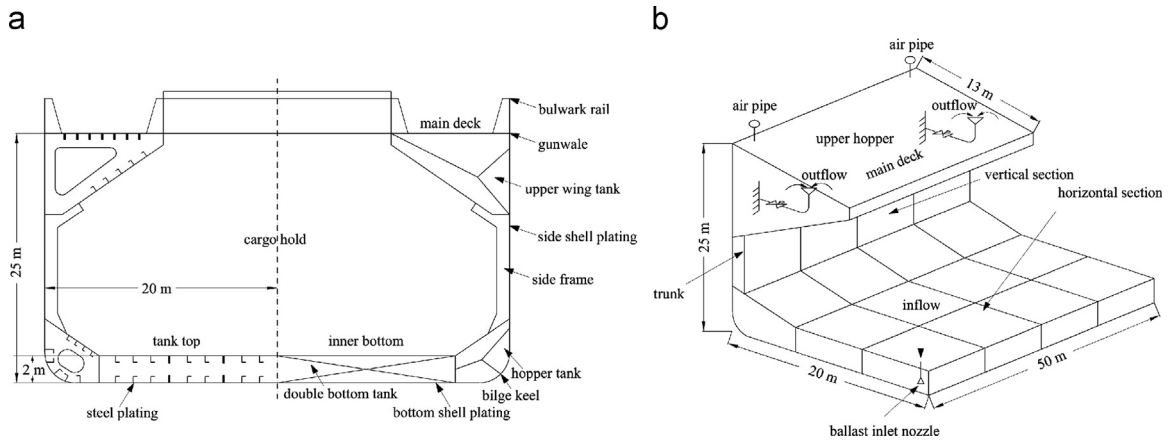

Fig. 1. Schematic drawings showing (a) oblique and (b) cross-section view of a ballast tank. The tanks are separated into port and starboard chambers (redrawn from Armstrong, 1997).

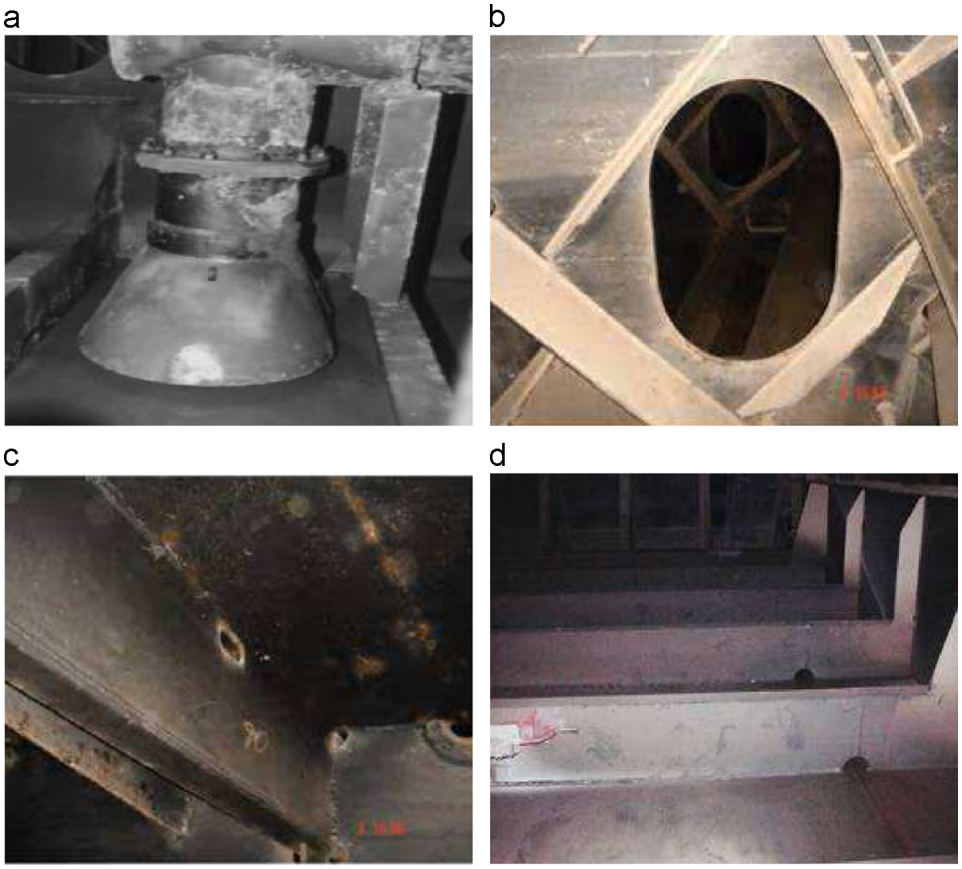

Fig. 2. Photographs of the interior geometry of a ballast tank showing (a) an inlet nozzle, (b) a lightening hole, (c) top limber holes, and (d) stringers with lower limber holes (taken from Steinhauer, 2007).

original water that is flushed out of the ballast tank can be used as a proxy for estimating the removal of NIS from the tanks. The current legislation deals with the number of exchange volumes that are required to achieve a level of flushing. Future treatment strategies are likely to do with reflushing and cleaning while the ship is in transit, and again, knowledge of the distribution of treated ballast water will be useful.

There are comparatively few theoretical studies of the flow within multi-compartment tanks. Wilson et al. (2006) and Chang et al. (2009) used CFD to examine the movement of fluid in a 1/3-scale double bottom tank and a full-scale ballast tank from a typical bulk carrier. When density contrast between the incoming seawater and the original freshwater was relatively large, the predicted flushing efficiency fell short of the required 95% replacement after three volumes exchange for both tanks, due to trappage in the tank tops. They found that the introduction of stringers encouraged plug flow where it might be expected that a more complex internal geometry would enhance mixing, and inferred that the addition of vent holes in the tank tops would allow for some movement of the trapped fluid. In the context of water treatment, Ta and Hague (2004) examined the flow through a multi-compartment ozone contactor, and achieved a mixed flow condition in the contact zone and a plug flow condition in the decay zone. However, due to the complexity of the calculations and long running time, it is difficult to implement CFD for practical design purposes (see Chu et al., 2009).

Meanwhile, there are few experimental studies of flow and flushing in ballast tanks. Kamada et al. (2004) measured the dilution rate of the fluid inside a two-dimensional square single tank using an optical method and also numerically analysed the fluid flow. After three exchange volumes by the flow through method, about 95% of the original fluid was removed. The influence of density contrast between the injected water and ballast water was examined by Eames et al. (2008) for a 'J'-type ballast tank with a planar geometry. In the absence of density contrast between the ballast water and that used to flush the tank, the high aspect ratio of tank geometry (along the base and the vertical sections) meant that a bulk Péclet number (based on a turbulent diffusivity) was high (>100) so that the transport out of the tank was largely through displacement. This is because the mixed interface between the incoming and the original fluid (perpendicular to the mean flow) was much smaller than the overall distance from the source and exit. Wilson et al. (2006) and Chang et al. (2009) tested a 1/3-scale 2×2 compartmented double bottom tank. When density contrast was large, there was still mostly unmixed original fluid trapped between the stringers near the tank tops after three volumes exchange. They found that decreasing the density contrast and increasing the inflow rate may improve mixing within the tank.

There are considerably more studies in a closely related area of air movement and ventilation within rooms and between rooms within buildings. Chen et al. (2010) assessed various types of models used to predict the ventilation performance in buildings. Many studies have focused on flow between rooms or boxes. Bolster and Linden (2007) examined flushing of contaminants from naturally ventilated rooms with comparison with Hunt and Kaye (2006), and found displacement ventilation may not be better than traditional mixing systems at removing contaminants. In the context of forced ventilation, Eames et al. (2009) examined the transient concentration of a continuous source of passive dye, which was injected into an acrylic model of a hospital isolation room. The measurement of the average concentration for the case of forced ventilation was in agreement with a simple model based on perfect mixing. Multizone transport models are an alternative to CFD models for investigating heat and pollutant transport in multi-room structure, which simplify the behaviour of spatially distributed physical systems into a topological network where nodes represent rooms/spaces and the connectors represent pathways. The system enables the average flow and mass transfer rate between different rooms based on the mass conservation and energy balance equations to approximate how materials or energies are transmitted among the compartments of the multibody fluid delivery system by assuming each room homogenous (see Chang et al., 2003). In the context of the ventilation literature, researchers dealt with an algebraic set of equations detailing the flux between rooms/windows with empirical closures for the pressure drop coefficients characterising the flow between spaces. For example, Zhao et al. (2003), Engdahl (1999) and Chu et al. (2009, 2010) have applied multizone models to simulate air velocity and temperature distributions in ventilated rooms.

Available methodologies to study ballast water exchange include field measurements, CFD, reduced models and small-scale experiments. Although field experiments are the most convincing method, they are expensive and restricted to specific types and therefore cannot provide general laws for all kinds of ships. For example, at three volumes flushing, the ballast water exchange efficiency is 99% for commercial oil tankers (Ruiz et al., 2005), 95% for bulk carriers (Rigby and Hallegraeff, 1994) and 87% for containerships (Ruiz and Reid, 2007). The dye samples were collected from the surface, 10 m deep and bottom of deck hatches. Due to limitations on tank access and sampling equipment, onboard experiments generally rely on measurements taken at the overflow outlet of the tank do not necessarily represent the volume mixture that remains in the ballast tank (Wilson et al., 2006). CFD can provide detailed results, but the major challenge is grid generation for such complex geometry and grid resolution. There is limited understanding of the vortex shedding flow due to the sharp edge of the lightening holes between compartments. The reduced mathematical model is restricted to simple flows, but time saving and easy to extend. The dimensionless groups characterising small-scale tests may not match those of field problems, which may restrict their applicability, but they tend to be easier to operate. Therefore, in this study a reduced model is developed and validated by laboratory scale experiments.

There is currently a significant gap in understanding how water that is initially in a ballast tank is removed by flushing. The purpose of this paper is to examine quantitatively how much of the initial water in idealised models of ballast tanks is removed using the current strategy of flushing. The focus in this paper is on scenarios where flushing occurs in waters with similar composition of the port water, where buoyancy effects are negligible. In the context of relatively closed systems, such as the Mediterranean and Baltic Seas, this assumption of uniform density is appropriate especially since the ballast water is taken at depths of 12 m beneath the free surface, similarly for seawater ports such as Singapore. For those ports near estuaries (e.g. Shanghai, New York, Hamburg, etc.), the change in density may be significant, this assumption is clearly not appropriate. In also trying to assess the influence of proposed cleaning technologies (ozone, UV, centrifugal separation), which are applied in transit, the density contrast between re-injected (cleaner) water and ballast water can be neglected. However, if ballast water is cleaned by heat, the treated water is lighter than the original water. The new element of the paper involves development of a robust multizone model for ballast water flushing and a detailed comparison against experimental results. To understand the influence of outlet arrangements and compartment configurations on the flushing efficiency, we examine the temporal and spatial fluid exchange experimentally.

The paper is structured as follows. In Section 2, we describe how we set up the mathematical model and the diagnostic tools used to interpret the results which are discussed in the context of simplified geometries; in Section 3, we apply the model on ballast tanks with different compartment configurations and outlet arrangements; in Section 4, we present the experimental setup and methodology; in

Section 5, we analyse the experimental results and compare with the model prediction; in Section 6, we conclude.

2. Mathematical model of multizone flow

The water used to flush a ballast tank is typically pumped into the tank at a rate $Q \sim 1\ \mathrm{m}^3/\mathrm{s}$. As we move farther away from the inlet nozzle, the mean flow decays quite quickly. It is important to estimate typical values as these variables determine the type of modelling approach and the validity of the experimental analogue described later. The ballast tanks in a large ship are characterised by a typical length $L=50$ m, width $W_h=20$ m of the base and $W_v=0.5$ m of the vertical region, height $H_h=2$ m of the horizontal region and $H_v=25$ m of the vertical region, and the nominal diameter of the inlet nozzle $D=0.5$ m. The mean flow velocity through the nozzle is $U_n = 4Q/(\pi D^2) \sim 5$ m/s. The flow in a ballast tank is characterised by the Reynolds number $Re = UL/\nu$, where ν is the kinematic viscosity of water, $\nu = 10^{-6}\ \mathrm{m}^2/\mathrm{s}$. We start using an assessment of the typical velocity and length scales in a ballast tank, where U and L are the characteristic velocity and lengthscale of the flow, respectively. The inlet nozzle Reynolds number is $Re_n = U_n D/\nu \sim 10^6$. Based on the horizontal section, $U_h \geq Q/(0.5\pi W_h H_h) \sim 10^{-2}$ m/s, $Re_h = U_h H_h/\nu \sim 10^4$. Up the riser section, $U_v = Q/(LW_v) \sim 10^{-2}$ m/s, so $Re_v = U_v W_v/\nu \sim 10^4$. Thus the flow in a ballast tank is inertially dominant so that Re is high and the flow is turbulent.

The purpose of this model is to quantify how flushing efficiency varies within a tank. The fraction of initial water that is flushed out of the tank serves as a useful metric of the ability of flushing to remove NIS. This can be estimated experimentally by dyeing the inlet water used for flushing and measuring the fraction of water in the tank which is dyed. Mathematically, this is equivalent to setting the dye water fraction as $C=0$ initially within the tank and $C=1$ on the inlet flow – the average of C over the tank represents a measure of the flushed fraction.

2.1. Mathematical modelling

The model assumptions are (a) the density difference between the inlet and the ballast water has a negligible effect dynamically, (b) the NIS are passive and (c) mixing within the compartments is perfect. The water exchange within the tank represents the removal of the NIS. Fig. 3(a) shows a schematic plan view of a general tank configuration consisting of m by n interconnected rectangular compartments, and the notation used in the mathematical model. The box structure of most ballast tanks means that this topological network (see Wu et al., 2012; Weinläder et al., 2012; Joekar-Niasar et al., 2010) is appropriate. This type of analysis is easily extendable to other topological networks. A compartment at the ith row and the jth column of the tank is referenced as $[i][j]$. The bottom right-hand corner compartment is the pipe entrance to the ballast tank, while the top left-hand and right-hand corner compartments are two outlets. The tank is not constrained to the horizontal plane and may 'fold' as it progresses from the double bottom of a ship up its sides. Water with the same density as the water in the tank is injected through the inlet. Fig. 3 (b) shows a schematic of a generic compartment within the ballast tank. $p_{[i][j]}$ is the pressure of compartment $[i][j]$. The volume flux from compartment $[i_1][j_1]$ to its neighbouring compartment $[i_2][j_2]$ (here $i_1 = i_2$, $|j_1 - j_2| = 1$ or $j_1 = j_2$, $|i_1 - i_2| = 1$) through an orifice with cross sectional area $A_{[i_1][j_1],[i_2][j_2]}$ is defined as

$$f_{[i_1][j_1],[i_2][j_2]} = \int_{A_{[i_1][j_1],[i_2][j_2]}} \boldsymbol{u} \cdot \hat{\boldsymbol{n}}\, \mathrm{d}A, \tag{1}$$

where $\boldsymbol{u}$ is the velocity, $\hat{\boldsymbol{n}}$ is a unit normal vector directed from compartment $[i_1][j_1]$ to compartment $[i_2][j_2]$. The fraction of water in compartment $[i][j]$ (of volume $V_{[i][j]}$) that has been flushed out is defined as

$$C_{[i][j]} = \frac{1}{V_{[i][j]}} \int_{V_{[i][j]}} C\, \mathrm{d}V. \tag{2}$$

The flushed fraction is calculated as a function of dimensionless time T, based on flushing the total tank volume (V), i.e.

$$T = \frac{Qt}{V}, \tag{3}$$

where $T=0$ corresponds to the tank starting to be flushed.

We develop a system of ordinary differential equations by integrating over individual compartments. The inertial force of the fluid is sufficiently large when compared to the buoyancy force so that the latter can be ignored. The basis of the model is that the incoming matter is well mixed and p is the same within each compartment, but the gradients of p and C between compartments

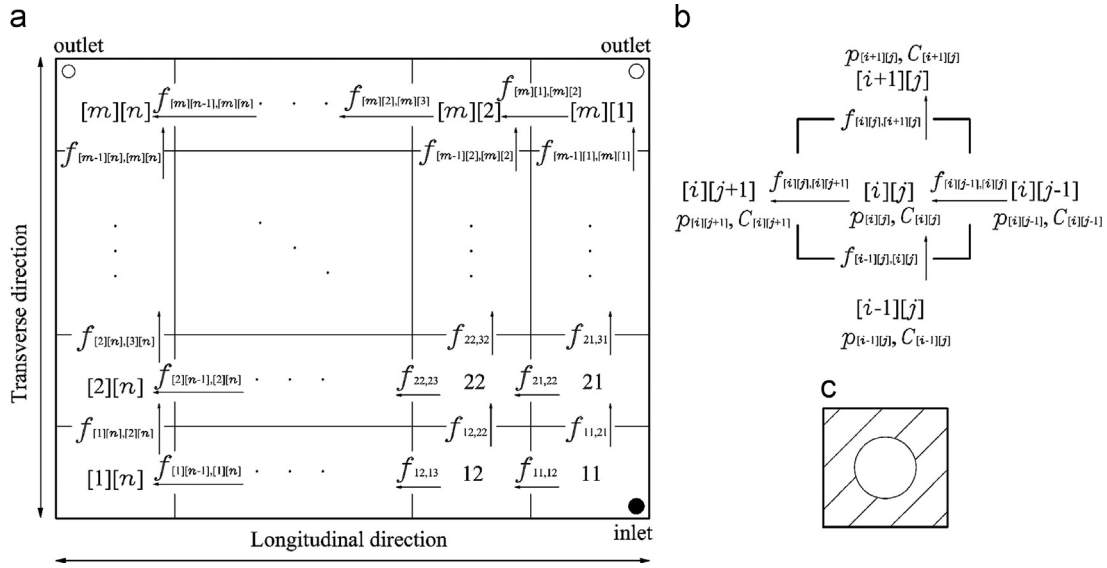

Fig. 3. Plan view of the configurations of (a) an $m \times n$ tank with one inlet and two outlets; (b) its generic compartment $[i][j]$ with notations of pressure, flushed fraction as well as flow rate; (c) a baffle with an orifice between two neighbouring compartments. Inlet is taken to be located in compartment 11 and two outlets are in compartments $[m][1]$ and $[m][n]$.

are important. Integrating the continuity equation over compartment $[i][j]$ gives

$$\sum f_{[i][j],\mathrm{in}} - \sum f_{[i][j],\mathrm{out}} = 0, \tag{4}$$

where $f_{[i][j],\mathrm{in}}$ and $f_{[i][j],\mathrm{out}}$ are the volume inflow rate and the volume outflow rate, respectively.

For steady flows, the multizone model of flow between compartments employs a semi-empirical closure model to relate the pressure drop with the average velocity through the holes. The approach adopted here is consistent with other studies (see Chu et al., 2009; Mora et al., 2003; Tan and Glicksman, 2005). The pressure difference between two neighbouring compartments $[i_1][j_1]$ and $[i_2][j_2]$ is

$$p_{[i_1][j_1]} - p_{[i_2][j_2]} = \xi_{[i_1][j_1],[i_2][j_2]} \rho \frac{|f_{[i_1][j_1],[i_2][j_2]}| f_{[i_1][j_1],[i_2][j_2]}}{A^2_{[i_1][j_1],[i_2][j_2]}}. \tag{5}$$

Here $\xi_{[i_1][j_1],[i_2][j_2]}$ is the local pressure loss coefficient between compartment $[i_1][j_1]$ and $[i_2][j_2]$, which is assumed to be constant. The pressure loss coefficient ξ is usually determined empirically. For instance, for flow through a sharp-edged circle orifice (see Cao et al., 2011; Charles et al., 2005; Chu et al., 2009) which is typical of the connection between compartments in ballast tanks, the pressure loss coefficient can be estimated by (Chu et al., 2010)

$$\xi = 2.58[1 - \exp(-60\beta)], \tag{6}$$

where β is the ratio of the cross-sectional area of the orifice to the cross-sectional area of the partition wall.

The fluid is transported by the mean flow and mixed by turbulent dispersion. The mean flow is largest in the passage between compartments and is smallest within compartments. Integrating the flushed fraction over compartment $[i][j]$, we have an approximate model describing the variation of the flushed fraction with time, i.e.

$$V_{[i][j]} \frac{\mathrm{d}C_{[i][j]}}{\mathrm{d}t} = \sum f_{[i][j],\mathrm{in}} C_{[i][j],\mathrm{in}} - \sum f_{[i][j],\mathrm{out}} C_{[i][j]}, \tag{7}$$

where $C_{[i][j],\mathrm{in}}$ is the flushed fraction in the compartment(s) flowing into compartment $[i][j]$. The general multizone model that consists of (4), (5) and (7) for an $m \times n$ tank is described in more detail in Appendix A.

2.2. Diagnostic tools

The mathematical model generates a time series for the flushed fraction of water in each compartment. A set of diagnostic tools are required to quantify the timescale when each compartment is flushed and the rate at which they are flushed by the incoming water. The dimensionless characteristic time $T_{1/2,[i][j]}$ for flushing is identified when half of the original fluid in compartment $[i][j]$ has been flushed out, mentioned as 'half flushed time'

$$T_{1/2,[i][j]} = T|_{C_{[i][j]} = 1/2}, \tag{8}$$

and $\alpha_{1/2,[i][j]}$ represents the characteristic flushing rate, at which compartment $[i][j]$ is being flushed when half of its original fluid has been flushed out (that is, when $T = T_{1/2,[i][j]}$)

$$\alpha_{1/2,[i][j]} = \frac{V_{[i][j]}}{V} \frac{\mathrm{d}C_{[i][j]}}{\mathrm{d}T}\Big|_{T = T_{1/2,[i][j]}}. \tag{9}$$

The flushing efficiency $\overline{C}$, is defined as the fraction of the original fluid that has been flushed out of the whole tank, i.e.

$$\overline{C}(T) = \frac{\sum_i \sum_j C_{[i][j]} V_{[i][j]}}{\sum_i \sum_j V_{[i][j]}}. \tag{10}$$

The diagnostics are applied to analyse the results from the multizone model and the experimental results.

3. Application of the model

We illustrate the effect of geometry on flushing by examining a series of tanks with increasing geometrical complexity from a 2×2, 3×3 to 5×4 tank. To build up a physical picture of the dynamics, we first analyse the simplest configuration – a four connected compartment arrangement with one inlet and two outlets, shown in Fig. 4(a). In order to simplify the analysis, we assume that the four compartments have the same shape and dimensions, and all the four holes between neighbouring compartments are the same thin-wall circular orifices in size, height and resistance. Similarly for the 3×3 case (see Fig. 4(b)), all the circular orifices between neighbouring compartments are geometrically congruent and same in height.

3.1. Application to a 2×2 tank

The solution is determined by four mass conservation equations by setting $m = n = 2$ in Appendix A:

$$f_{11,12} + f_{11,21} = Q, \quad f_{11,12} = f_{12,22}, \quad f_{11,21} = f_{21,22} + Q_{21,\mathrm{out}}, \quad f_{12,22} + f_{21,22} = Q_{22,\mathrm{out}}; \tag{11}$$

and four empirical closures for the pressure drop:

$$p_{11} - p_{12} = \xi_{11,12} \rho \frac{|f_{11,12}| f_{11,12}}{A^2_{11,12}}, \quad p_{21} - p_{22} = \xi_{21,22} \rho \frac{|f_{21,22}| f_{21,22}}{A^2_{21,22}},$$
$$p_{11} - p_{21} = \xi_{11,21} \rho \frac{|f_{11,21}| f_{11,21}}{A^2_{11,21}}, \quad p_{12} - p_{22} = \xi_{12,22} \rho \frac{|f_{12,22}| f_{12,22}}{A^2_{12,22}}. \tag{12}$$

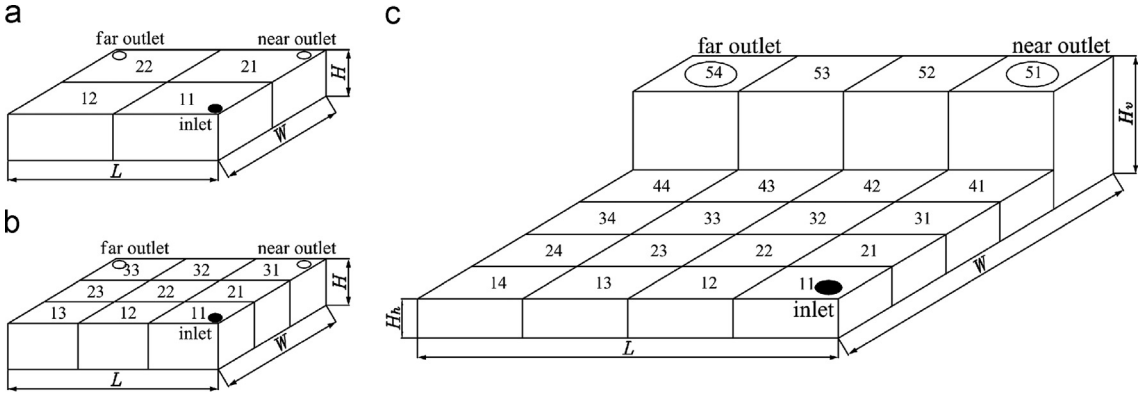

Fig. 4. Elevated schematic of a (a) 2×2 square tank, (b) 3×3 square tank, and (c) 5×4 'J'-type tank with one inlet and two outlets. The inlet and outlets on the top of the tanks are indicated.

In this example, we consider the influence of outlet arrangement on flushing where the geometry of the lightening holes is the same. Here $\xi_{11,12}=\xi_{21,22}=\xi_{11,21}=\xi_{12,22}$ and $A_{11,12}=A_{21,22}=A_{11,21}=A_{12,22}$. When only the far outlet is open ($Q_{21,\mathrm{out}}=0$, $p_{22}=0$), the solution to the equation array is

$$f_{11,12}=f_{11,21}=f_{12,22}=f_{21,22}=\frac{Q}{2},\quad Q_{22,\mathrm{out}}=Q; \tag{13}$$

when only the near outlet is open ($Q_{22,\mathrm{out}}=0$, $p_{21}=0$), after manipulation, the solution is

$$f_{11,12}=f_{12,22}=\frac{(\sqrt{3}-1)Q}{2},\quad f_{21,22}=\frac{(1-\sqrt{3})Q}{2},\quad f_{11,21}=\frac{(3-\sqrt{3})Q}{2},$$
$$Q_{21,\mathrm{out}}=Q; \tag{14}$$

when both outlets are open ($p_{21}=p_{22}=0$), the fluxes between the compartments are

$$f_{11,12}=f_{12,22}=Q_{22,\mathrm{out}}=(\sqrt{2}-1)Q,\quad f_{21,22}=0,$$
$$f_{11,21}=Q_{21,\mathrm{out}}=(2-\sqrt{2})Q. \tag{15}$$

The flushed fraction in each compartment evolves according to the following:

$$\frac{\mathrm{d}C_{11}}{\mathrm{d}T}=\frac{V}{V_{11}}(1-C_{11}),$$
$$\frac{\mathrm{d}C_{12}}{\mathrm{d}T}=\frac{V}{V_{12}}\left(\frac{f_{11,12}}{Q}C_{11}-\frac{f_{12,22}}{Q}C_{12}\right),$$
$$\frac{\mathrm{d}C_{21}}{\mathrm{d}T}=\frac{V}{V_{21}}\left(\frac{f_{11,21}}{Q}C_{11}-\frac{f_{21,22}}{Q}(H(f_{21,22})C_{21}+H(-f_{21,22})C_{22})-\frac{Q_{21,\mathrm{out}}}{Q}C_{21}\right),$$
$$\frac{\mathrm{d}C_{22}}{\mathrm{d}T}=\frac{V}{V_{22}}\left(\frac{f_{12,22}}{Q}C_{12}+\frac{f_{21,22}}{Q}(H(f_{21,22})C_{21}+H(-f_{21,22})C_{22})-\frac{Q_{22,\mathrm{out}}}{Q}C_{22}\right), \tag{16}$$

and satisfies the initial condition

$$C_{[i][j]}|_{T=0}=0.$$

The Heaviside function (where $H(X)=1$ for $X\geq 0$ and $H(X)=0$ for $X<0$) is needed to prevent flow in the wrong direction.

The system of coupled linear differential equations can be solved analytically and the solution for $V_{[i][j]}/V=1/4$ is given in Appendix B. The curves in Fig. 5 show the predicted flushed fraction variation in each compartment of the 2×2 tank for the three cases considered. In all cases, C_{22} is the slowest to be flushed as a consequence of being the farthest from the inlet. For the 'far open' case, the symmetry in the flow pathways means that $C_{12}=C_{21}$. For the 'near open' case, there is a crossover between C_{12} and C_{21}. This is because while $f_{11,21}>f_{11,12}$ leads to an initially faster increase in C_{21}, at a later time, the fluid with a lower flushed fraction is being transported from compartment 22 to 21 leading to $C_{12}>C_{21}$. For the 'both open' case, the flow largely passes through compartment 21 as $C_{21}>C_{12}$.

Fig. 6(a–c;i) summarises the characteristic flushing rate versus the half flushed time in each of the compartments. In all cases, $\alpha_{1/2,11}=1/2$, $T_{1/2,11}=\ln 2/4$ since the compartments are all the same size. The increases for compartments 12 and 21 are quite similar in all cases. While from Fig. 6(b,i), compartment 12 is ultimately flushed slightly faster than 21, the values of $\alpha_{1/2}$, $T_{1/2}$ do not capture this because they describe the initial characteristics of flushing. Compartment 22 is flushed at similar rates in both the 'near open' and 'both open' cases.

3.2. Application to a 3×3 tank

As the number of compartments increases, the complexity of the dynamics increases. The predictions of the variation of the flushed fraction in compartments 12, 13, 22 and 23 of the 3×3 tank are shown by the curves in Fig. 7. For all the three outlet arrangements, $C_{12}>C_{22}>C_{13}>C_{23}$. Compartment 12 is flushed in a similar manner for the three cases because the flux through these compartments is weakly dependent on the global influence of the boundary condition. Compared with 'far open', compartments 13, 22 and 23 for the 'near open' case are flushed more slowly. For the 'both open' case, these compartments are flushed more slowly than those for 'far open', but faster than those for 'near open'. The model predicted characteristic flushing rate versus the half flushed time for each compartment is shown in the left of Fig. 8. In all cases, compartment 11 is characterised by $\alpha_{1/2,11}=1/2$ and $T_{1/2,11}=\ln 2/9$. For the 'far open' case, due to the symmetry of the flow, $\alpha_{1/2,12}=\alpha_{1/2,21}$, $\alpha_{1/2,13}=\alpha_{1/2,31}$, and $\alpha_{1/2,23}=\alpha_{1/2,32}$ (see Fig. 8(a,i)). Compartment 33 is always flushed at a slower rate than all the other compartments. The farther a compartment is from the inlet, the more slowly it is flushed. From Fig. 8(b,i), it can be seen that there are three groups of accumulated points: compartments 21 and 12, compartments 31, 22 and 13, and compartments 32 and 23. In general, compartments are half flushed at a later time in the 'both open' case than in the 'far open' case, but earlier than those in the 'near open' case.

3.3. Application to a 5×4 tank

Fig. 4(c) shows a schematic of a 5×4 tank which consists of compartments which have a rectangular footprint, and holes between neighbouring compartments are not the same in size and number (see Table 1). The resistance coefficients used to close the system of equations were estimated using (6). The theoretical predictions of the variation of the flushed fraction field are shown in Fig. 9(a–c;i). For all the three outlet arrangements, the tank is flushed from the right bottom to the left top. At $T=0.25$, the difference of the fraction field among these three cases is not significant. But at a later time, the tank is most efficiently flushed for the 'far open' case, and more original fluid remains on the left corner compartments for the 'near open' case. The predictions of the characteristic flushing rate versus the half flushed time for each compartment are shown in the left of Fig. 10. The points donating $\alpha_{1/2}$ versus $T_{1/2}$ are grouped into two parts associated with the equal sized horizontal compartments (the first to the fourth rows of the tank) and the larger vertical compartments (the fifth row). The horizontal compartments behave similarly for each case, because the global character of the flushing depends more weakly on the outlet arrangement as the number of compartments increases. In general, the nearer a compartment is located to the inlet, the faster and earlier it is flushed, leading to a bow-shaped decrease of the scatter plot of $\alpha_{1/2,[i][j]}$ versus $T_{1/2,[i][j]}$ (see Fig. 10(a–c;i)). For all cases, $T_{1/2,11}=\ln 2V_{11}/V$, $\alpha_{1/2,11}=1/2$. For a large number of compartments, we expect that the flow is 'radial' for short time where $u_r\sim 2Q/\pi r H_h$, where r is the distance from the inlet. This gives an approximate relation $\alpha_{1/2}\sim T_{1/2}^{-1}$, which is confirmed by plotting Fig. 10 on a log–log scale. The relative positions of the points denoting the vertical compartments to those for the horizontal compartments are different for different outlet arrangements. The vertical compartments are flushed more slowly and later in the 'both open' case than in the 'far open' case, but faster and earlier than in the 'near open' case.

3.4. Flushing efficiency of the tanks

The flushing efficiency in the whole tank (defined by (10)) is shown in the left of Fig. 11 for the three tanks, and compared against the pure displacement and perfect mixing. For each case, the flushing

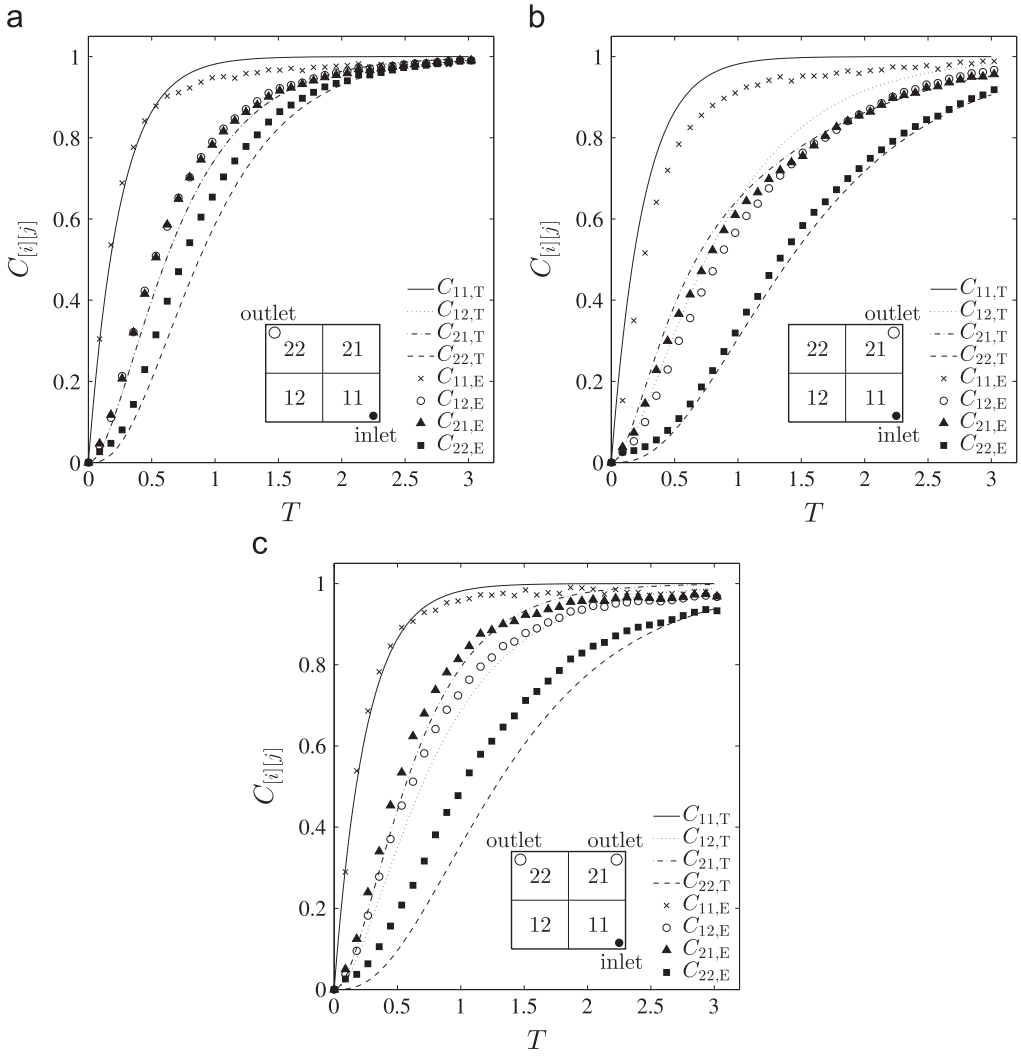

Fig. 5. The theoretical predictions and the corresponding experimental measurements of the flushed fraction variation in each compartment of a 2×2 tank. $C_{[i][j],T}$ represents theoretical predictions, while $C_{[i][j],E}$ represents experimental measurements. The figures correspond to (a) 'far open', (b) 'near open', and (c) 'both open' cases.

efficiency is intermediated between the pure displacement and perfect mixing. Table 2 summarises the flushing efficiency at $T=3$. For all the three tanks, the flushing efficiency is the highest in the 'far open' case, and the lowest in the 'near open' case. This is because when the outlet is placed far from the inlet, the incoming fluid has more chance to mix with the initial fluid and thus the latter can be replaced more efficiently. Also, it can be seen that when a tank is divided into many compartments, the flow behaves like the displacement mode, as the incoming fluid will leave the tank when it has mixed more sufficiently with the initial fluid (except for some 'near open' cases). Therefore, subdividing a ballast tank would improve the total flushing efficiency. The critical point is that for all the tanks considered, the flushing efficiency is greater than 95% at three exchange volumes ($T=3$) that is required by the IMO protocols. The model predictions will be compared against laboratory scale experiments.

4. Experimental study

A series of experiments were undertaken to provide a means of testing quantitatively the capability of the flushing model to capture the exchange processes in multi-compartment tanks. We studied the flushing processes in a 2×2, 3×3 and 5×4 tank. To reduce the number of variables, the flow rate was fixed to examine different outlet arrangements for each compartment configuration.

4.1. Experimental apparatus

Two acrylic model tanks were employed in the experimental study. The geometric scale ratio is 50. One was a square tank of width 61 cm and height 20 cm, shown in Fig. 12(a and b). Three PVC pipes with valves were inserted through the cover into the tank as potential inlets, and on the other side of the cover, another three PVC pipes were inserted into the tank as potential outlets. Clamps and sealing trips were used to give a water tight seal to the tank. To generate the 2×2 and 3×3 internal configurations, six plates in total were employed, each of which was 61 cm long, 20 cm high and 1 cm thick. There was a 10 cm long and 1 cm thick gap in the middle of each plate, so that the two plates each of which has two circular holes could be crossed each other and inserted into the tank to generate the 2×2 internal configuration (see Fig. 12(a)) and the other four plates each of which has three circular holes could be crossed each other to generate the 3×3 internal configuration (see Fig. 12(b)). All these circular holes had a diameter of 10 cm and located in the middle height between two neighbouring compartments. The tank volume is 75 l.

The second was a 'J'-type tank consisting of 5×4 compartments with one inlet and two outlets, which was designed based on the typical geometry of a ballast tank (see Fig. 12(c)). The orifices between compartments in the longitudinal and transverse directions were different. This tank was characterised by a horizontal section

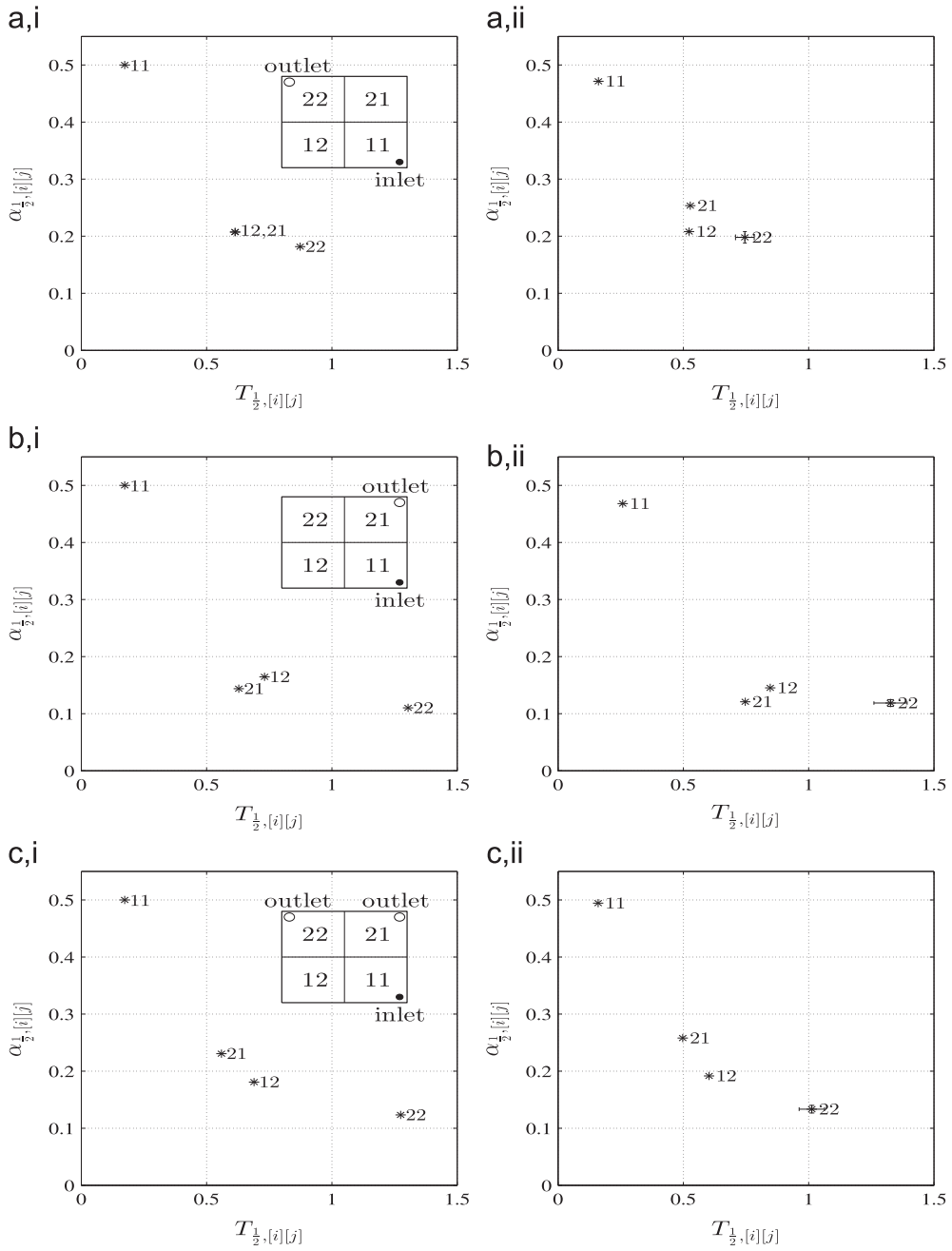

Fig. 6. The theoretical predictions of the scatter plot $\alpha_{1/2}$ versus $T_{1/2}$ in each compartment are shown on the left (i), with the corresponding experimental results on the right (ii) for a 2×2 tank. The figures correspond to (a) 'far open', (b) 'near open', and (c) 'both open' cases. The bar on point 22 gives an indication of the experimental error.

(double bottom tank), turning section (hopper tank), internal geometry with longitudinal and transverse frames, the filling pipes and two overflow arrangements with fixed height. Semicircular limber holes were added at the top and bottom of each interconnecting wall of width and depth 0.8 cm. The model tank was designed to be geometrically complex, the detailed structure and dimensions of which are listed in Table 1. Water was pumped in through a 2-cm diameter hole at the ceiling of the horizontal section, and exited from funnels fixed at height 28 cm of the tank. The total volume of the tank is 75 l: each of the 16 horizontal compartments has a volume of 2.5 l, and the volume of compartments 51, 52, 53 and 54 is 8 l, 9.5 l, 9.5 l and 8 l, respectively.

The acrylic models were placed in a large tank and illuminated by a uniform diffuse light source placed beneath; an inclined mirror was placed above the tank to obtain the plan view (see Fig. 12(c)).

4.2. Experimental procedure

For each tank configuration, similar to the theoretical study, three outlet arrangements were considered: 'far open', 'near open', and 'both open'. The inflow rate was fixed at Q=0.25 l/s, which is the maximum flow rate we can achieve accurately in our laboratory. For both tanks, the Reynolds number at the nozzle exit was $Re_n \sim 8000$. At some corner compartments, $Re \sim 1000$ for the square tank, $Re \sim 600$ for the 'J'-type tank.

At the start of each experiment, the tank was filled with clear water, and then a dilute methylene blue dye solution (concentration of 0.1 mg/l) was pumped into the tank via the inlet. Images were taken at a rate of 7.5 frames per second by an Allied Vision Dolphin machine vision and saved as a BMP file every 100 frames. Matlab Image Processing Toolbox was employed to analyse these images.

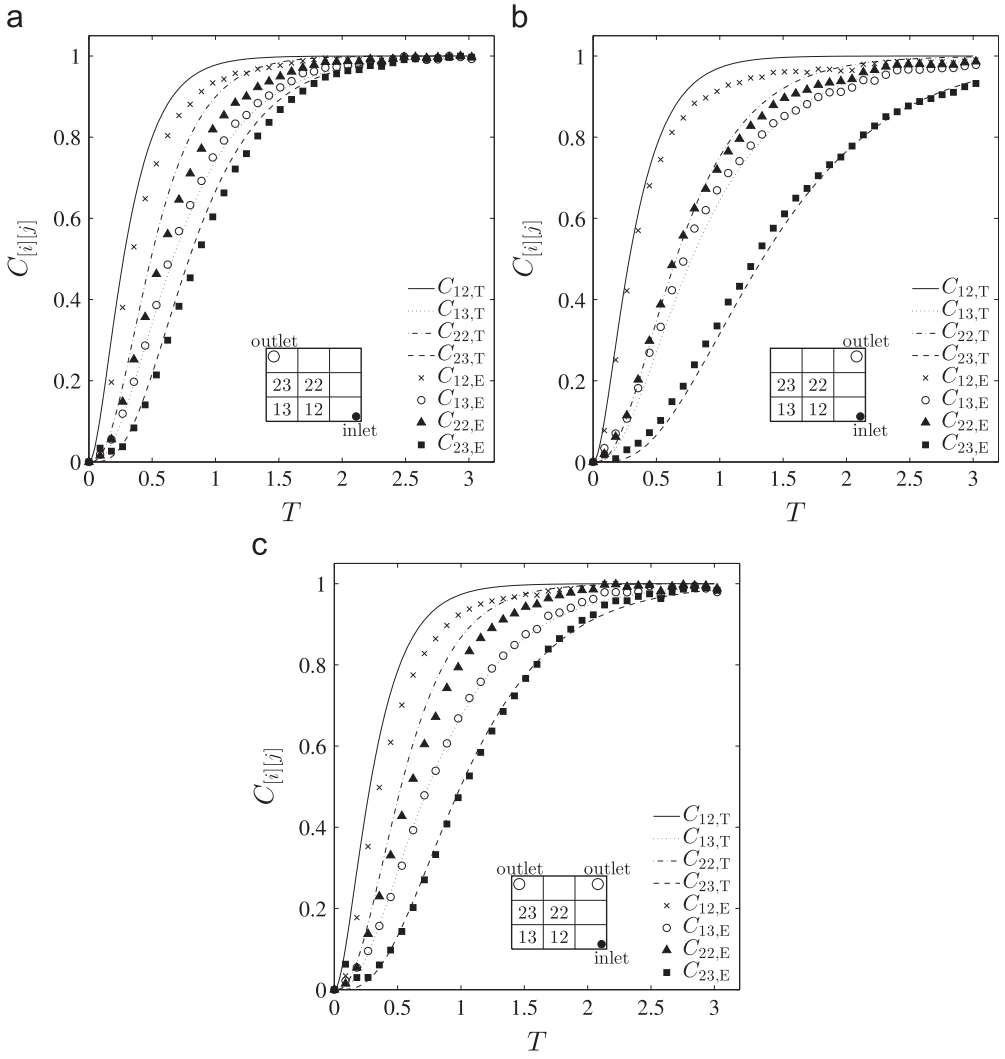

Fig. 7. The theoretical predictions and the corresponding experimental measurements of the flushed fraction variation in four selected compartments of the 3 × 3 tank. $C_{[i][j],T}$ represents theoretical predictions, while $C_{[i][j],E}$ represents experimental measurements. The figures correspond to (a) 'far open', (b) 'near open', and (c) 'both open' cases.

4.3. Experimental principle and analytical tools

The experiments involved measuring the fraction of initial water in each compartment that is flushed out when water is injected into the tank. With the help of the inclined mirror, the camera captured a plan view of the tank. Dye water was injected into the tank (see Kamada et al., 2004). An optical method was used to assess the mass of dye within each compartment based on the classical absorption theory of Lambert–Beer (see Cenedese and Dalziel, 1998; Rahim et al., 2010; Zeng et al., 2010; Suhling et al., 2001). The image processing was based on the principle that the depth integrated dye concentration in water can be related to the intensity of light passing through the water and the distance travelled by the light in the water. The dye concentration in the water at point (x,y) can then be related to the change in light intensity through

$$C_I(x,y) = \int_0^l C(x,y,z)\mathrm{d}z = f\left(\log\frac{I_0(x,y)}{I(x,y)}\right), \tag{17}$$

where l is the distance in the z-direction that the light travels in the water, I_0 is the light intensity after the light travels through clear water, and I is the light intensity after the light travels through dye water. The function $f(x)$ is determined by a series of calibration tests for fixed l. The volume averaged flushed fraction in compartment $[i][j]$ is

$$C_{[i][j]}(T) = \frac{\int_{A_{[i][j]}} C_I \,\mathrm{d}A}{\int_{A_{[i][j]}} C_{I,\eta}\,\mathrm{d}A}, \tag{18}$$

where $C_{I,\eta}$ is the depth integrated dye concentration when compartment $[i][j]$ is completely filled with dye water, calculated from (17), and $A_{[i][j]}$ is the base area of compartment $[i][j]$.

The main point was to determine the fraction of initial fluid in each compartment that is removed, as a function of time. The diagnostic tools defined in Section 2.2 to analyse the model predictions were applied to analyse the experimental data. For images captured from the experiments, each compartment from the plan view was individually masked so that its time series (18) could be evaluated.

We estimated $T_{1/2,[i][j]}$ by interpolating $C_{[i][j]}$ to determine when $C_{[i][j]} = 0.5$. We estimated $\alpha_{1/2,[i][j]}$ by linearly regressing $C_{[i][j]}$ with T over the interval $|C_{[i][j]} - 0.5| \le 0.1$ and identified $\alpha_{1/2,[i][j]}$ proportional to the slope of the curve.

4.4. Experimental errors

The major experimental measurement errors are caused by masking and calibration. From a series of calibration tests, a

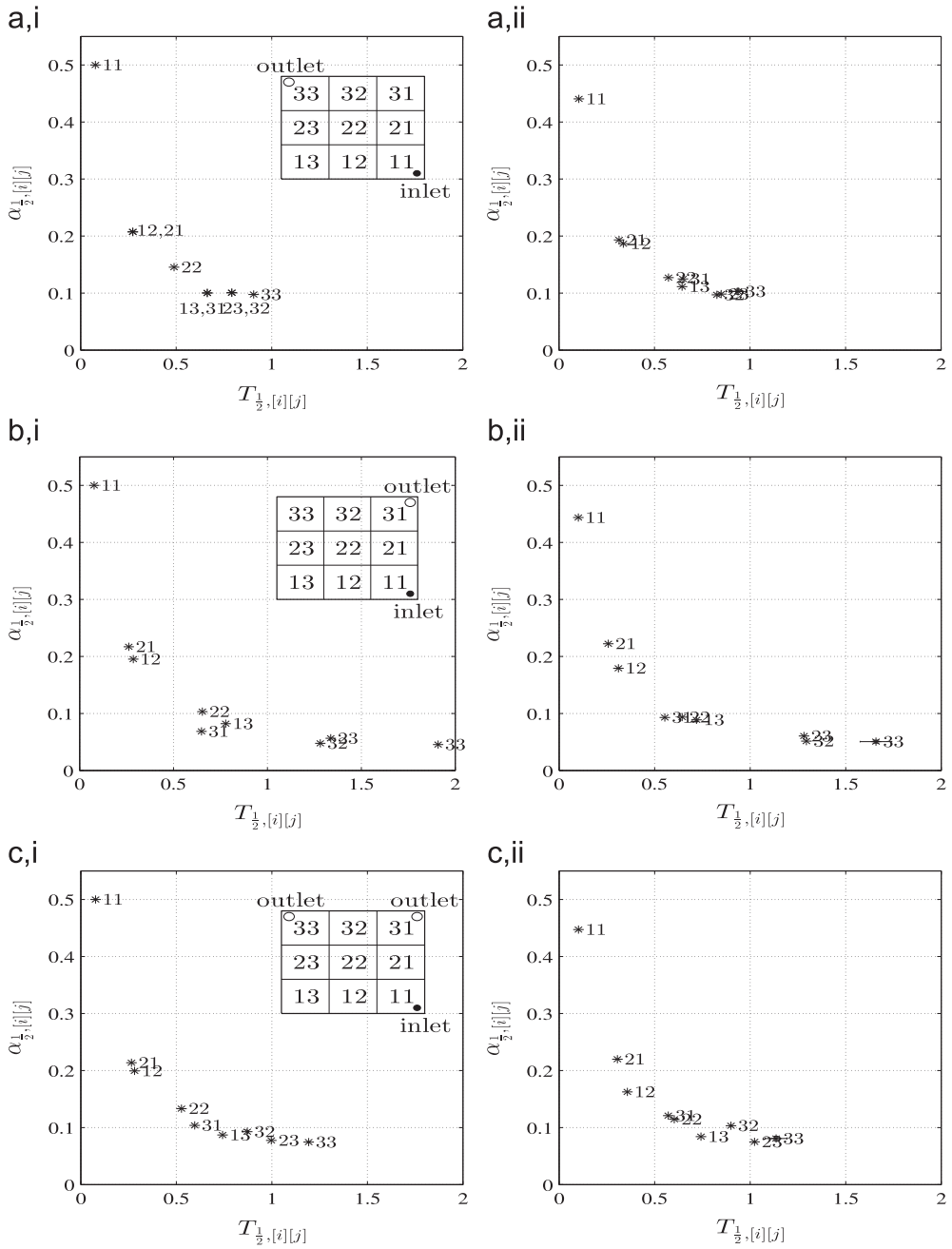

Fig. 8. The theoretical predictions of the scatter plot $\alpha_{1/2}$ versus $T_{1/2}$ in each compartment are shown on the left (i), with the corresponding experimental results on the right (ii) for a 3×3 tank. The figures correspond to (a) 'far open', (b) 'near open', and (c) 'both open' cases. The bar on point 33 gives an indication of the experimental error.

Table 1
The structure and dimensions of the 5×4 tank used in the experiment.

Item	Horizontal section	Vertical section
Row number	4	1
Column number	4	4
Compartment length (cm)	25	25
Compartment width (cm)	10	13
Compartment height (cm)	10	30
Number of lightening holes	Longitudinal 1	3
between two compartments	Transverse 2	
Diameter of lightening holes (cm)	5	8

standard error of 2% was observed in relating dye concentration to light intensity. On the top and bottom of the tank, lack of transparency in some points may decrease the measured dye concentration by about 1%. The compartments of the tank are individually assessed by masking part of the total image. The compartments have dimensions of around 100×100 pixels; masking is accurate to within 10 pixels and thus gives an error of 1%. During the pumping and flushing, small bubbles attached to the wall that form due to temperature change inside the tank may lead to a maximum error of 1%. In total, the experimental measurements have an error less than 5%.

5. Experimental results

The experimental results reveal the characteristics of ballast water exchange in the 2×2, 3×3 and 5×4 compartment configurations, with a steady inflow rate. We will see how these experimental results match the model predictions.

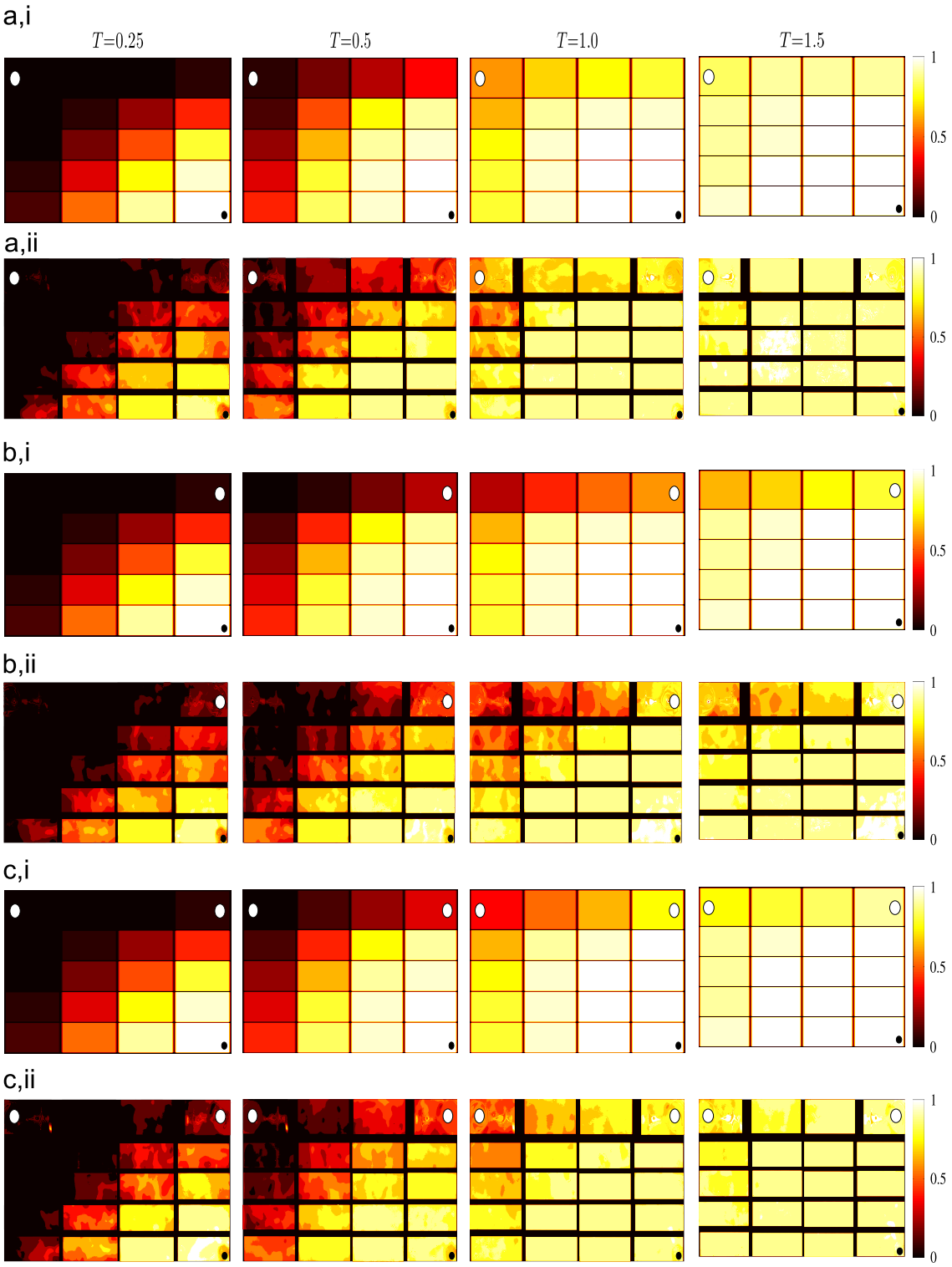

Fig. 9. The theoretical predictions of the flushed fraction field in each compartment of the 5×4 tank at $T=0.25$, 0.5, 1 and 1.5 are shown in the upper row (i) of (a–c), with the corresponding experimental measurements in the lower row (ii). The figures correspond to (a) 'far open', (b) 'near open', and (c) 'both open' cases. A black circle represents an inlet, and a white circle represents an outlet.

5.1. 2×2 tank

The scatter plots in Fig. 5 show the experimental measurements of how the flushed fraction in each compartment of the 2×2 tank, $C_{[i][j]}$, varied in time for the 'far open', 'near open' and 'both open' cases. The results compare quite well with the model predictions. For all cases, C_{11} grew the fastest, C_{22} the most slowly, while C_{12} and C_{21} lay between C_{11} and C_{22}. From Fig. 5(a) for the 'far open' case, C_{12} and C_{21} behaved nearly the same, which is expected due to the inherent symmetry of the flow; from Fig. 5 (b) for 'near open', C_{21} grew faster from the beginning, until $T \approx 1.3$ when it was exceeded by C_{12}; from Fig. 5(c) for 'both open', C_{21} was always higher than C_{12} was. For the 'both open' case, C_{22} is underestimated because we assume that $p_{21} = p_{22}$. In

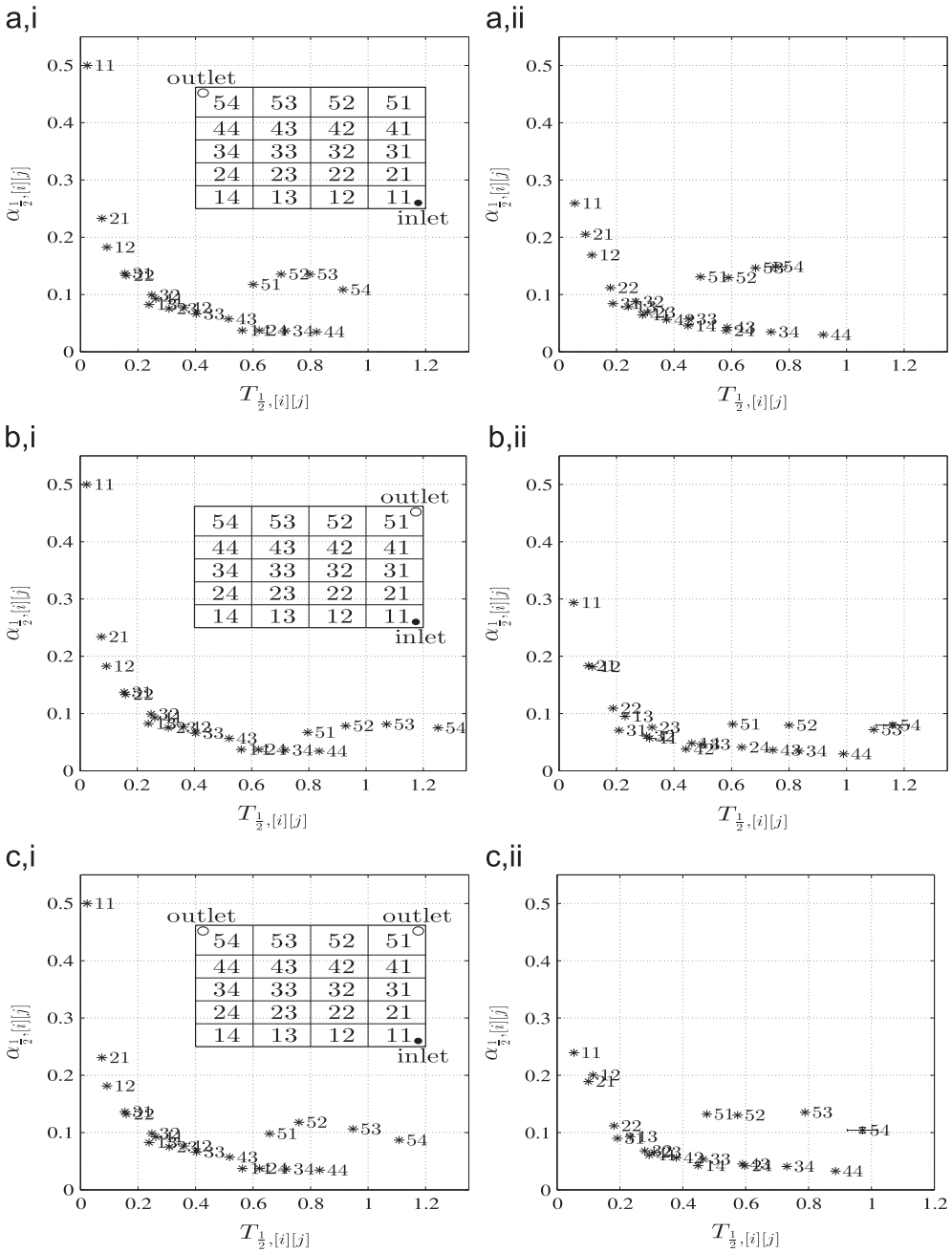

Fig. 10. The theoretical predictions of the scatter plot $\alpha_{1/2}$ versus $T_{1/2}$ in each compartment are shown on the left (i), with the corresponding experimental results on the right (ii) for a 5×4 tank. The figures correspond to (a) 'far open', (b) 'near open', and (c) 'both open' cases. The bar on point 54 gives an indication of the experimental error.

fact, there existed a small flow from compartment 21 to 22, which accelerated the increase of C_{22}. Meanwhile, from Fig. 6(a–c;ii), the corresponding $\alpha_{1/2,[i][j]}$ versus $T_{1/2,[i][j]}$ matched the model predictions. Overall, the experimental results were in close agreement with the model predictions for the 2×2 tank.

5.2. 3×3 tank

The scatter plots in Fig. 7 show the experimental measurements of the flushed fraction in the four selected compartments of the 3×3 tank as a function of time. For all cases, C_{12} and C_{22} are a little overestimated. The agreement with the values of $\alpha_{1/2,[i][j]}$ versus $T_{1/2,[i][j]}$ (see Fig. 8) is quite good, although for all cases, compartment 11 was flushed a little more slowly than expected. The probable reason is that the incoming fluid had not completely mixed with the original fluid in the compartment when it left, that is, the existence of orifices between neighbouring compartments challenged the perfect mixing assumption within each compartment; compartment 11 was the first and fastest flushed compartment, so its flushing rate was influenced most severely by the non-perfect mixing condition. For the 'near open' case, the model successfully predicted the three grouped points: 12 and 21; 22, 13 and 31; and 23 and 32 (see Fig. 8(b)). Overall, the experimental results captured the main character of the flushing predicted by the model. The measurements of the flushed fractions were consistent with the model predictions on the performance of the four selected compartments. Meanwhile, the characteristic flushing rate and the half flushed time predicted by the model for each compartment of the tank were validated by the experiments for the three outlet arrangements.

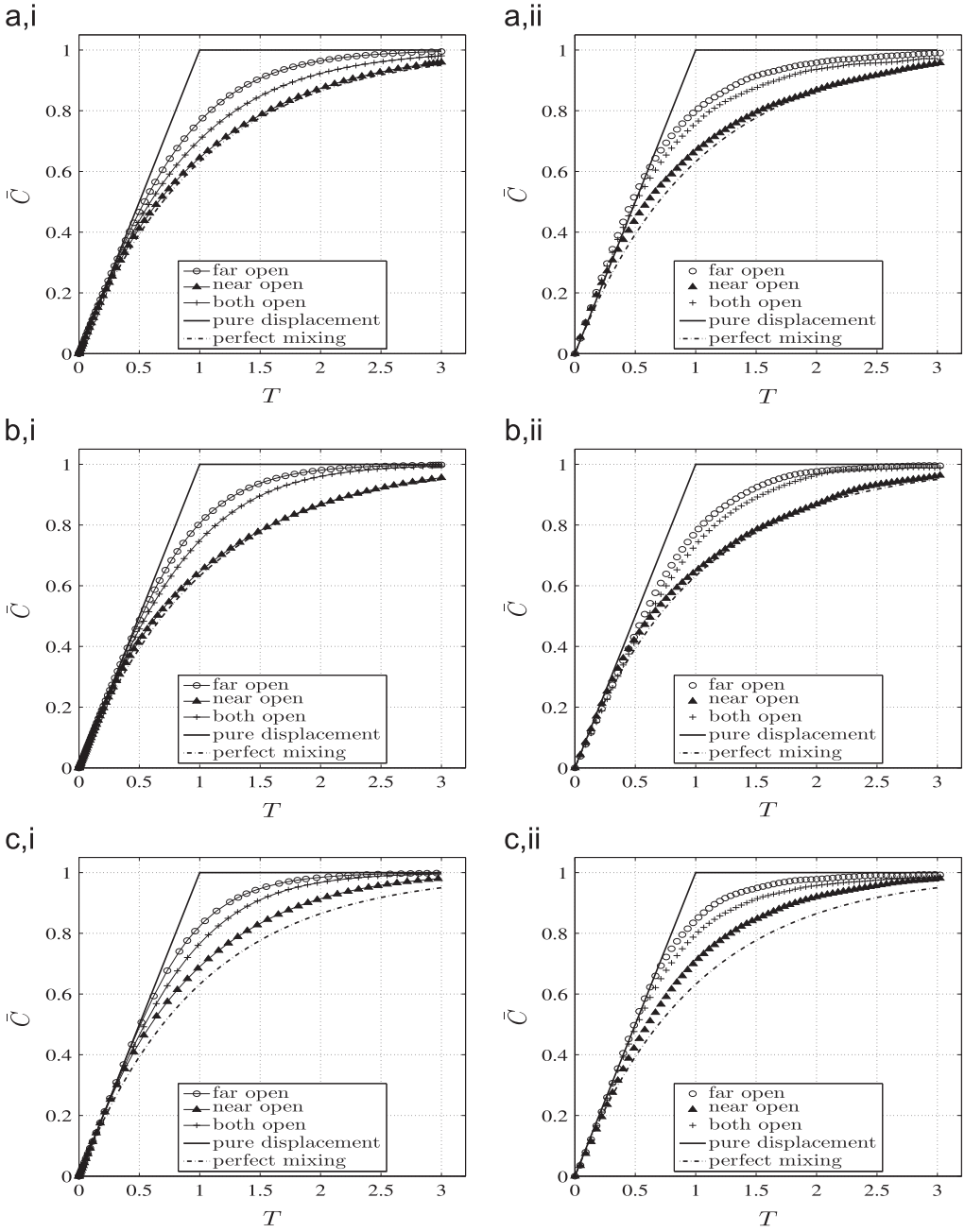

Fig. 11. The theoretical predictions of the flushing efficiency of the whole tanks with three outlet arrangements are shown on the left (i), with the corresponding experimental results on the right (ii). The figures correspond to the (a) 2×2, (b) 3×3, and (c) 5×4 tanks.

Table 2
The theoretical and experimental flushing efficiencies at $T=3$ of the tanks with different compartment configurations and outlet arrangements.

Compartment configuration	Theoretical/experimental flushing efficiency (%)		
	Far open	Near open	Both open
2×2	99.5/99.0	96.0/95.7	98.1/97.2
3×3	99.8/99.6	95.6/96.4	99.4/98.4
5×4	99.9/99.3	98.1/97.9	99.6/98.5

5.3. 5×4 tank

The model predictions and experimental measurements of the variation of the flushed fraction field are shown in Fig. 9. The experimental results agreed well with the model predictions. At an early time, the performance of each compartment was not significantly different among different outlet arrangements; at a later time, the residual fluid was the least for the 'far open' case, but the most for the 'near open' case. The bow-shaped decrease of $\alpha_{1/2,[i][j]}$ versus $T_{1/2,[i][j]}$ in Fig. 10(a–c;ii) indicated that the farther a compartment was from the inlet, the more slowly and later it was half flushed. $\alpha_{1/2,11}$ was more underestimated than that in the 3×3 tank. The probable reason is that the perfect mixing assumption of the model was challenged when the ratio of the orifice area to the partition wall area between compartments (β) was too large. When the area of the hole of a compartment to its neighbouring compartment was too large, the incoming water could not mix sufficiently with the original water when it left the compartment. In our tests, $\beta=19.6$–38.6% for the 5×4 tank, which was much larger than that of the 2×2 tank ($\beta=13.1\%$) and the

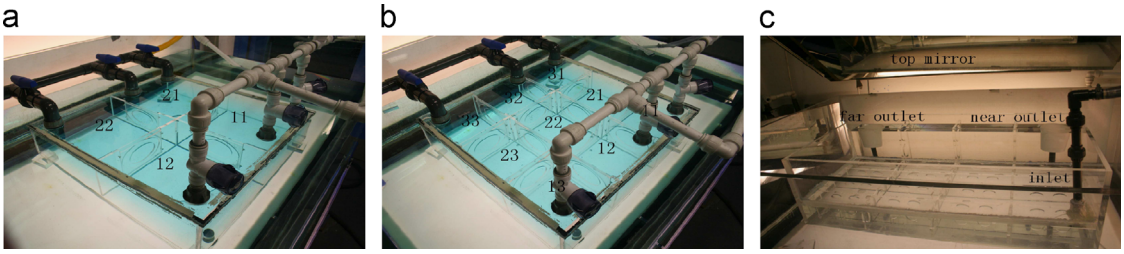

Fig. 12. Photograph of the (a) 2×2 square tank, (b) 3×3 square tank, and (c) 5×4 'J'-type tank used in the experimental study.

3×3 tank ($\beta=4.91\%$). In real ballast tanks, the ratio is normally less than 15%. A possible reason for the longer residence of the original water in some compartments (e.g. compartment 44) for the 'near open' and 'both open' cases is that the flux in the peripheral compartments decreased to $\sim 0.2Q$, giving a characteristic Reynolds number of $Re \simeq 600$, so that the turbulence was weak, leading to insufficient mixing and high residence times for fluid parcels in the recirculating region attached to the outlet holes. Compartments 21 and 12 were half flushed at relatively high rates, their neighbouring compartments 31, 22 and 13 were flushed at lower rates, and other horizontal compartments were then half flushed at even lower rates. It can be seen that the relative position of the points denoting the vertical compartments to those denoting the horizontal compartments agreed with the predictions. The model is able to capture the variation of the flushed fraction of each compartment with time and discern the performance difference of each compartment among the three outlet arrangements.

5.4. Flushing efficiency of the whole tanks

The variation of the tank flushing efficiency with time is shown in the right of Fig. 11. It can be found that for a short time, the original fluid was removed by displacement and the increase in $\overline{C}$ was roughly linear; for a long time, mixing was important and then $\overline{C}$ followed more closely the perfect mixing rule. For all tank configurations the flushing efficiencies of 'far open' and 'both open' were similar and higher than that of the 'near open' case. For the 'far open' and 'both open' cases, the flushing efficiency increased linearly with time up until $T\simeq0.6$, because the water exiting consisted entirely of water that was initially in the tank. When $T\gtrsim0.6$, the water exiting the tank consisted of an increasing fraction of the water that was being used for flushing the tank. In total, the flushing efficiency at $T=3$ of these two cases was lower than the pure displacement, but higher than estimates based on perfect mixing in the whole tank. For the 'near open' case, the transition from displacement flushing to mixing occurred earlier at $T\simeq0.5$, because the incoming water bypassed a large part of the tank and was not able to exchange the initial water efficiently. Table 2 summarises the flushing efficiency at $T=3$ for each case. Generally, the flushing efficiency at $T=3$ obtained from the experiments was slightly lower than predicted, except for the 'near open' case in the 3×3 tank. In these experiments, the effective Re decreased in the peripheral compartments leading to lower increase rates of flushed fraction and higher residence time. Since the total flushing efficiency is an integrated measure over the whole tank, the impact of the peripheral compartments is not significant and this is why the agreement between the theory and the experiments is generally good. The discrepancy between the model predictions and the experimental measurements for $\overline{C}|_{T=3}$ is within 1.1%, lower than the limit of experimental errors $\sim5\%$. Therefore, the model is able to understand how the flushing efficiency depends on the outlet arrangements and tank geometries.

6. Discussion and conclusion

In this paper, we have examined theoretically and experimentally the flushing of water from a multi-compartment ballast tank. The model is based on perfect mixing within compartments and advection between compartments. To test the model predictions, a series of detailed experiments on tanks with 2×2 and 3×3 compartment configurations were undertaken. When the lightening holes between compartments are identical, the model has no adjustable free parameters, and the agreement between the measurements of the flushed fraction of water in each compartment and predictions is quite good. When the holes between compartments of a tank are different in size, an empirical closure is required to estimate pressure drop coefficients.

The flushing from a tank with more complex geometry, typical of a ballast tank, was also analysed. The agreement between predictions and measurements for the flushing efficiency is good. The increased complexity means that the flow through the edge compartments is reduced and in the laboratory study, probably to the extent that the flow within these regions was not turbulent. Insufficient mixing, caused by weak turbulent diffusion in some compartments where the flow rate was low, led to a long residence time of the original fluid and thus a slow exchange, that is why the American Bureau of Shipping (2010) requires that aft and fore peak tanks are to be provided with additional pipework to improve the mixing conditions.

The IMO requires that after three exchange volumes, the flushing efficiency should be greater than 95% and these estimates were based on a perfect mixing model for the whole tank. The theoretical model and experiments show that for homogeneous fluids within multi-compartment tanks, flushing is more efficient than estimated by the IMO, and can be improved by subdividing the tanks. The results show that to enhance flushing the outlet should be placed far from the inlet to reduce bypassing, which is consistent with the requirement by the American Bureau of Shipping. There is currently no guidance about where the water in the ballast tanks should be sampled. This is not trivial because there are usually multiple discharge ports. And as we see in the flushed fraction curves there is a significant variability between compartments and the validated theoretical framework in this paper will go some way to assessing tanks in practice.

The current analysis is applicable to cases when the initial ballast water and the water used for flushing have the same density. There are a number of scenarios where the density contrast may be important (e.g. using a heat treatment to sterilise the water or ports in warm shallow seas or near fresh water sources). Some initial insight can already be obtained for a line of connected compartments (e.g. Eames et al., 2008) but further work is required to extend this analysis to more realistic geometries. More work is needed to extend the model to account for the settling and sticking dynamics of non-passive substances. A number of authors have included this effect by the inclusion of a sink term in the mass conservation equation (e.g. Eq. (13) of

Bolster and Linden, 2009) $-v_T A_{[i][j]} C_{[i][j]}/h$ (where v_T is the terminal fall velocity) on the right-hand side of (7).

Acknowledgement

The Erasmus Mundus External Cooperation Programme financed by the European Commission is acknowledged.

Appendix A. Mathematical model for an $m \times n$ tank

The ballast tank for this study from the plan view has m rows by n columns compartments with a steady flow rate Q into compartment 11. There are two outlets, with flow rate $Q_{[m][1],\mathrm{out}}$ out of compartment $[m][1]$ and $Q_{[m][n],\mathrm{out}}$ out of compartment $[m][n]$, respectively. To mathematically study this ballast tank following the way of the above analysis, it is abstracted as a model in Fig. 3. The model consists of mn mass conservation equations:

$$
\begin{aligned}
&Q = f_{11,12} + f_{11,21},\\
&f_{[1][n-1],[1][n]} = f_{[1][n],[2][n]},\\
&f_{[m-1][1],[m][1]} = f_{[m][1],[m][2]} + Q_{[m][1],\mathrm{out}},\\
&f_{[m-1][n],[m][n]} + f_{[m][n-1],[m][n]} = Q_{[m][n],\mathrm{out}},\\
&f_{[1][j-1],[1][j]} = f_{[1][j],[1][j+1]} + f_{[1][j],[2][j]}, \quad j = 2,3,\ldots,n-1,\\
&f_{[m][j-1],[m][j]} + f_{[m-1][j],[m][j]} = f_{[m][j],[m][j+1]}, \quad j = 2,3,\ldots,n-1,\\
&f_{[i-1][1],[i][1]} = f_{[i][1],[i][2]} + f_{[i][1],[i+1][1]}, \quad i = 2,3,\ldots,m-1,\\
&f_{[i-1][n],[i][n]} + f_{[i][n-1],[i][n]} = f_{[i][n],[i+1][n]}, \quad i = 2,3,\ldots,m-1,\\
&f_{[i-1][j],[1][j]} + f_{[i][j-1],[i][j]} = f_{[i][j],[i][j+1]} + f_{[i][j],[i+1][j]}, \quad i = 2,3,\ldots,m-1\\
&\quad \text{and} \quad j = 2,3,\ldots,n-1;
\end{aligned}
\tag{A.1}
$$

and $2mn-m-n$ momentum equations:

$$
p_{[i][j]} - p_{[i][j+1]} = \xi_{[i][j],[i][j+1]} \rho \frac{|f_{[i][j],[i][j+1]}| f_{[i][j],[i][j+1]}}{A^2_{[i][j],[i][j+1]}}, \quad i = 1,2,\ldots,m \quad \text{and}
$$

$$
j = 1,2,\ldots,n-1;
$$

$$
p_{[i][j]} - p_{[i+1][j]} = \xi_{[i][j],[i+1][j]} \rho \frac{|f_{[i][j],[i+1][j]}| f_{[i][j],[i+1][j]}}{A^2_{[i][j],[i+1][j]}},
$$

$$
i = 1,2,\ldots,m-1 \quad \text{and} \quad j = 1,2,\ldots,n. \tag{A.2}
$$

When only the far outlet is open, $Q_{[m][1],\mathrm{out}} = 0$, $p_{[m][n]} = 0$; when only the near outlet is open, $Q_{[m][n],\mathrm{out}} = 0$, $p_{[m][1]} = 0$; when both outlets are open, $p_{[m][1]} = p_{[m][n]} = 0$. The equations describing the variation of the flushed fraction in time are

$$
\begin{aligned}
\frac{dC_{11}}{dT} &= \frac{V}{V_{11}}(1 - C_{11}), \frac{dC_{[1][n]}}{dT}\\
&= \frac{V}{V_{[1][n]}}\left(\frac{f_{[1][n-1],[1][n]}}{Q} C_{[1][n-1]} - \frac{f_{[1][n],[2][n]}}{Q} C_{[1][n]}\right),
\end{aligned}
$$

$$
\begin{aligned}
\frac{dC_{[m][1]}}{dT} = \frac{V}{V_{[m][1]}}\Bigg(&\frac{f_{[m-1][1],[m][1]}}{Q} C_{[m-1][1]} - \frac{f_{[m][1],[m][2]}}{Q}\left(H(f_{[m][1],[m][2]}) C_{[m][1]}\right.\\
&\left. + H(-f_{[m][1],[m][2]}) C_{[m][2]}\right) - \frac{Q_{[m][1],\mathrm{out}}}{Q} C_{[m][1]}\Bigg),
\end{aligned}
$$

$$
\begin{aligned}
\frac{dC_{[m][n]}}{dT} = \frac{V}{V_{[m][n]}}\Bigg(&\frac{f_{[m-1][n],[m][n]}}{Q} C_{[m-1][n]}\\
&+ \frac{f_{[m][n-1],[m][n]}}{Q}\left(H(f_{[m][n-1],[m][n]}) C_{[m][n-1]}\right.\\
&\left. + H(-f_{[m][n-1],[m][n]}) C_{[m][n]}\right) - \frac{Q_{[m][n],\mathrm{out}}}{Q} C_{[m][n]}\Bigg),
\end{aligned}
$$

$$
\frac{dC_{[1][j]}}{dT} = \frac{V}{V_{[1][j]}}\left(\frac{f_{[1][j-1],[1][j]}}{Q} C_{[1][j-1]} - \frac{f_{[1][j],[2][j]}}{Q} C_{[1][j]} - \frac{f_{[1][j],[1][j+1]}}{Q} C_{[1][j]}\right),
$$

$$
j = 2,3,\ldots,n-1,
$$

$$
\begin{aligned}
\frac{dC_{[m][j]}}{dT} = \frac{V}{V_{[m][j]}}\Bigg(&\frac{f_{[m][j-1],[m][j]}}{Q}\left(H(f_{[m][j-1],[m][j]}) C_{[m][j-1]}\right.\\
&\left. + H(-f_{[m][j-1],[m][j]}) C_{[m][j]}\right)\\
&+ \frac{f_{[m-1][j],[m][j]}}{Q} C_{[m-1][j]} - \frac{f_{[m][j],[m][j+1]}}{Q}\left(H(f_{[m][j],[m][j+1]}) C_{[m][j]}\right.\\
&\left. + H(-f_{[m][j],[m][j+1]}) C_{[m][j+1]}\right)\Bigg), \quad j = 2,3,\ldots,n-1,
\end{aligned}
$$

$$
\begin{aligned}
\frac{dC_{[i][1]}}{dT} = \frac{V}{V_{[i][1]}}\Bigg(&\frac{f_{[i-1][1],[i][1]}}{Q} C_{[i-1][1]} - \frac{f_{[i][1],[i][2]}}{Q}\left(H(f_{[i][1],[i][2]}) C_{[i][1]}\right.\\
&\left. + H(-f_{[i][1],[i][2]}) C_{[i][2]}\right) - \frac{f_{[i][1],[i+1][1]}}{Q} C_{[i][1]}\Bigg), \quad i = 2,3,\ldots,m-1,
\end{aligned}
$$

$$
\begin{aligned}
\frac{dC_{[i][n]}}{dT} = \frac{V}{V_{[i][n]}}\Bigg(&\frac{f_{[i-1][n],[i][n]}}{Q} C_{[i-1][n]} + \frac{f_{[i][n-1],[i][n]}}{Q}\left(H(f_{[i][n-1],[i][n]}) C_{[i][n-1]}\right.\\
&\left. + H(-f_{[i][n-1],[i][n]}) C_{[i][n]}\right) - \frac{f_{[i][n],[i+1][n]}}{Q} C_{[i][n]}\Bigg),
\end{aligned}
$$

$$
i = 2,3,\ldots,m-1,
$$

$$
\begin{aligned}
\frac{dC_{[i][j]}}{dT} = \frac{V}{V_{[i][j]}}\Bigg(&\frac{f_{[i][j-1],[i][j]}}{Q}\left(H(f_{[i][j-1],[i][j]}) C_{[i][j-1]} + H(-f_{[i][j-1],[i][j]}) C_{[i][j]}\right)\\
&+ \frac{f_{[i-1][j],[i][j]}}{Q} C_{[i-1][j]} - \frac{f_{[i][j],[i][j+1]}}{Q}\left(H(f_{[i][j],[i][j+1]}) C_{[i][j]}\right.\\
&\left. + H(-f_{[i][j],[i][j+1]}) C_{[i][j+1]}\right) - \frac{f_{[i][j],[i+1][j]}}{Q} C_{[i][j]}\Bigg),
\end{aligned}
$$

$$
i = 2,3,\ldots,m-1 \quad \text{and} \quad j = 2,3,\ldots,n-1 \tag{A.3}
$$

along with

$$
C_{[i][j]}|_{T=0} = 0.
$$

Here $H(X)$ is the Heaviside step function with the properties $H(X) = 1$ for $X \geq 0$ and $H(X) = 0$ for $X < 0$.

Appendix B. Analytical solutions to $C_{[i][j]}$ of a 2×2 tank

For the case of a 2×2 tank, where the flux between each compartment is known, the flushed fraction can be explicitly determined from (16) for the case of $V_{[i][j]}/V = 1/4$. For the 'far open' case,

$$
\begin{aligned}
&C_{11} = 1 - \exp(-4T),\\
&C_{12} = 1 - 2\exp(-2T) + \exp(-4T),\\
&C_{21} = 1 - 2\exp(-2T) + \exp(-4T),\\
&C_{22} = 1 - 4\exp(-2T) + (4T+3)\exp(-4T);
\end{aligned}
\tag{B.1}
$$

for the 'near open' case,

$$
\begin{aligned}
&C_{11} = 1 - \exp(-4T),\\
&C_{12} = 1 - \frac{\sqrt{3}+3}{3}\exp((2-2\sqrt{3})T) + \frac{\sqrt{3}}{3}\exp(-4T),\\
&C_{21} = 1 - \frac{12T+\sqrt{3}-3}{9}\exp((2-2\sqrt{3})T)\\
&\qquad + \frac{(12\sqrt{3}-48)T+\sqrt{3}-12}{9}\exp(-4T),\\
&C_{22} = 1 - \frac{4\sqrt{3}T+2}{3}\exp((2-2\sqrt{3})T) - \frac{1}{3}\exp(-4T);
\end{aligned}
\tag{B.2}
$$

for the 'both open' case,

$$
\begin{aligned}
&C_{11} = 1 - \exp(-4T),\\
&C_{12} = 1 - \frac{\sqrt{2}+2}{2}\exp((4-4\sqrt{2})T) + \frac{\sqrt{2}}{2}\exp(-4T),\\
&C_{21} = 1 - (\sqrt{2}+1)\exp((4\sqrt{2}-8)T) + \sqrt{2}\exp(-4T),\\
&C_{22} = 1 - \frac{4\sqrt{2}T+1}{2}\exp((4-4\sqrt{2})T) - \frac{1}{2}\exp(-4T).
\end{aligned}
\tag{B.3}
$$

References

American Bureau of Shipping, 2010. Guide for Ballast Water Exchange.

Armstrong, G., 1997. Ballast system design for flow-through exchange of ballast water. Trans. IMarE. 109, 257–269.

Bolster, D.T., Linden, P.F., 2007. Contaminants in ventilated filling boxes. J. Fluid Mech. 591, 97–116.

Bolster, D.T., Linden, P.F., 2009. Particle transport in low-energy ventilation systems. Part 2: transients and experiments. Indoor Air 19, 130–144.

Cao, R., Liu, Y.S., Yan, C., 2011. A criterion for flow mechanisms through vertical sharp-edged orifice and model for the orifice discharge coefficient. Petrol. Sci. 8 (1), 108–113.

Cenedese, C., Dalziel, S.B., 1998. Concentration and depth field determined by the light transmitted through a dyed solution. In: Eighth International Symposium on Flow Visualization, pp. 1–5.

Chang, III, P.A., Wilson, W., Carneal, J., Atsavapranee, P., Verosto, S., Reid, D., Jenkins, P., 2009. Computational modeling of ballast water tanks to improve understanding and maximize effectiveness of management practices and treatment mechanisms. Phase ii—Extension of Laboratory Study (Final Report). Technical Report, NOAA Technical Memorandum GLERL-148, National Oceanic and Atmospheric Administration, Great Lakes Environmental Research Laboratory, Ann Arbor, MI, and NSWCCD-50-TR-2009/028, Naval Surface Warfare Center Carderock Division, West Bethesda, MD, USA.

Chang, T.J., Huang, M.Y., Wu, Y.T., Liao, C.M., 2003. Quantitative prediction of traffic pollutant transmission into buildings. J. Environ. Sci. Health A 38 (6), 1025–1040.

Charles, S., Bonneau, O., Frene, J., 2005. Determination of the discharge coefficient of a thin-walled orifice used in hydrostatic bearings. J. Tribol. 127 (3), 679–684.

Chen, Q.Y., Lee, K., Mazumdar, S., Poussou, S., Wang, L.Z., Wang, M., Zhang, Z., 2010. Ventilation performance prediction for buildings: model assessment. Build. Environ. 45 (2), 295–303.

Chu, C.R., Chiu, Y.H., Chen, Y., Wang, Y.W., Chou, C.P., 2009. Turbulence effects on the discharge coefficient and mean flow rate of wind-driven cross-ventilation. Build. Environ. 44 (10), 2064–2072.

Chu, C.R., Chiu, Y.H., Wang, Y.W., 2010. An experimental study of wind-driven cross ventilation in partitioned buildings. Energ. Build. 42 (5), 667–673.

Eames, I., Landeryou, M., Greig, A., Snellings, J., 2008. Continuous flushing of contaminants from ballast water tanks. Mar. Pollut. Bull. 56 (2), 250–260.

Eames, I., Shoaib, D., Klettner, C.A., Taban, V., 2009. Movement of airborne contaminants in a hospital isolation room. J. R. Soc. Interface 6, 757–766.

Engdahl, F., 1999. Stability of mechanical exhaust systems. Indoor Air 9 (4), 282–289.

Hunt, G.R., Kaye, N.B., 2006. Pollutant flushing with natural displacement ventilation. Build. Environ. 41 (9), 1190–1197.

Joekar-Niasar, V., Hassanizadeh, S.M., Dahle, H.K., 2010. Non-equilibrium effects in capillarity and interfacial area in two-phase flow: dynamic pore-network modelling. J. Fluid Mech. 655, 38–71.

Kamada, K., Minami, K., Shoji, K., Shiotani, S., Ishida, H., 2004. Study of ballast water exchange by pumping-through method. In: Oceans '04 MTS/IEEE Techno-Ocean '04, vols. 1–2, Conference Proceedings, vols. 1–4, pp. 707–712.

King, D.M., Hagan, P.T., Riggio, M., Wright, D.A., 2012. Preview of global ballast water treatment markets. J. Mar. Eng. Technol. 11 (1), 3–16.

MacPhee, B., 2006. Alien flotillas: the expansion of invasive species through ship ballast water. In: EarthTrends Environmental Essay Competition Winner, pp. 1–8.

Magill, S.H., Thetmeyer, H., Cromey, C.J., 2006. Settling velocity of faecal pellets of gilthead sea bream (*sparus aurata* l.) and sea bass (*dicentrarchus labrax* l.) and sensitivity analysis using measured data in a deposition model. Aquaculture 251, 295–305.

Mora, L., Gadgil, A.J., Wurtz, E., 2003. Comparing zonal and CFD model predictions of isothermal indoor airflows to experimental data. Indoor Air 13 (2), 77–85.

Pimentel, D., Lach, L., Zuniga, R., Morrison, D., 2000. Environmental and economic costs of nonindigenous species in the United States. BioScience 5, 53–65.

Rahim, R.A., Rahiman, M.H.F., Goh, C.L., Muji, S.Z.M., Rahim, H.A., Yunos, Y.M., 2010. Modeling orthogonal and rectilinear mixed-modality projection of optical tomography for solid-particles concentration measurement. Sensor. Actuat. A: Phys. 161 (1–2), 53–61.

Rigby, G., Hallegraeff, G., 1994. The transfer and control of harmful marine organisms in shipping ballast water: behaviour of marine plankton and ballast water exchange trials on the mv 'iron whyalla". J. Mar. Environ. Eng. 1, 91–110.

Ruiz, G.M., Murphy, K.R., Verling, E., Smith, G., Chaves, S., Hines, A.H., 2005. Ballast water exchange: efficacy of treating ships' ballast water to reduce marine species transfers and invasion success? Technical Report. Report Submitted to Prince William Sound Regional Citizens' Advisory Council and the US Fish & Wildlife Service, 14p.

Ruiz, G.M., Reid, D.F., 2007. Current state of understanding about the effectiveness of ballast water exchange (bwe) in reducing aquatic nonindigenous species (ans) introductions to the great lakes basin and chesapeake bay, USA: synthesis and analysis of existing information. Technical Report. National Oceanic and Atmospheric Administration, United States Department of Commerce.

Steinhauer, F., 2007. Ballast water exchange and the destruction of non-indigeneous species (Master's thesis). University College London.

Suhling, K., Hungerford, G., Airey, R.W., Morgan, B.L., 2001. A position-sensitive photon event counting detector applied to fluorescence imaging of dyes in sol–gel matrices. Meas. Sci. Technol. 12 (2), 131–141.

Ta, C.T., Hague, J., 2004. A two-phase computational fluid dynamics model for ozone tank design and troubleshooting in water treatment. Ozone-Sci. Eng. 26 (4), 403–411.

Tan, G., Glicksman, L., 2005. Application of integrating multi-zone model with CFD simulation to natural ventilation prediction. Energ. Build. 37 (10), 1049–1057.

Weinläder, A., Wu, W., Tenbohlen, S., Wang, Z., 2012. Prediction of the oil flow distribution in oil-immersed transformer windings by network modelling and computational fluid dynamics. IET Electr. Power Appl. 6, 82–90.

Wilson, W., Chang, P., Verosto, S., Atsavapranee, P., Reid, D.F., Jenkins, P.T., 2006. Computational and experimental analysis of ballast water exchange. Nav. Eng. J. 118 (3), 25–36.

Wong, K.B., Piedrahita, R.H., 2000. Settling velocity characterization of aquacultural solids. Aquacult. Eng. 21, 233–246.

Wonham, M.J., Carlton, J.T., 2005. Trends in marine biological invasions at local and regional scales: the northeast Pacific Ocean as a model system. Biol. Invasions 7, 369–392.

Wright, D.A., 2012. Logistics of compliance assessment and enforcement of the 2004 ballast water convention. J. Mar. Eng. Technol. 11 (1), 17–24.

Wright, D.A., Mackey, T.P., 2006. Shipboard and dockside trials of ballast water treatment technology. Nav. Eng. J. 118 (3), 37–43.

Wu, W., Wang, Z.D., Revell, A., Jarman, P., 2012. Computational fluid dynamics calibration for network modelling of transformer cooling flows. Part ii: pressure loss at junction nodes. IET Electr. Power Appl. 6, 28–34.

Zeng, N.Y., Li, Y.R., Du, M., 2010. Rapid quantitative image analysis of hCG by gold immunochromatographic assay and genetic fast FCM algorithm. In: Third International Conference on Biomedical Engineering and Informatics, pp. 1560–1564.

Zhao, B., Li, X.T., Yan, Q.S., 2003. A simplified system for indoor air flow simulation. Build. Environ. 38 (4), 543–552.